Secondary instabilities in all fiber ring cavities

Zheng Liu,[1] François Leo,[2,3] Saliya Coulibaly,[1,*] and Majid Taki[1]

[1]*PhLAM, Université de Lille 1, Bâtiment P5-bis, UMR CNRS/USTL 8523, F-59655 Villeneuve d'Ascq, France*

[2]*Service OPERA-photonique, Université libre de Bruxelles (U.L.B.), 50 Avenue F. D. Roosevelt, Code Postal 194/5, B-1050 Bruxelles, Belgium*

[3]*Photonics Research Group, Department of Information Technology, Ghent University-IMEC, Ghent B-9000, Belgium*

(Received 15 October 2013; revised manuscript received 18 June 2014; published 22 September 2014)

We study secondary instabilities in a coherently driven passive optical fiber cavity. We show that time-modulated solutions which are generated at the onset of instability experience convective and absolute Eckhaus instabilities. The splitting of the secondary instabilities into convective and absolute instabilities drastically impacts the instability boundaries. As a consequence, the stability range of time-modulated waves is enlarged. More importantly, the threshold of absolute instability determines the transition from time-periodic wave trains to a chaotic regime. In the latter the wave trains are composed of irregular oscillations embedded in regular ones. The predictions are in excellent agreement with numerical simulations.

DOI: 10.1103/PhysRevA.90.033837 PACS number(s): 42.65.Sf, 42.55.Tv, 42.55.Wd, 42.81.−i

I. INTRODUCTION

There is currently a considerable interest in understanding the nonlinear dynamics in optical fiber cavities that belong to the class of nonequilibrium dissipative systems. It is well known that the latter experience different generic instability characteristics of nonlinear dynamical systems, namely, the ones modeled by partial differential equations. This concerns almost all fields in science ranging from chemical reactions, biology, to nonlinear optics and fluid mechanics [1]. In optics, the formation of dissipative solutions (DSs) arises naturally in many optical devices from the coupling of dispersion (temporal systems) or diffraction (spatial systems), nonlinearities, and dissipation. This coupling triggers various spatiotemporal instabilities, which lead to spontaneous formation of DSs that can be stationary or not, periodic, or localized in the form of dissipative solitons [2]. Among the possible devices, coherently driven optical fiber ring cavities have recently appeared as one of the most promising systems, not only for the richness in their nonlinear dynamics [3] but also for their potential applications [4]. It has been shown that, in the presence of third-order dispersion, the standard theoretical approach leading to modulation instability must be extended [5,6]. More specifically, a nonlinear stationary state may be unstable with respect to localized perturbations, but the state that results will depend on the relative values of the amplification and the drift induced by the third-order dispersion term. This is the basis of the difference between convective and absolute regimes. In the former, the perturbation grows in time but decreases locally because it is advected away. In the latter it increases locally and not only in the moving frame, so it eventually extends over all the slow time domain. In this case, threshold values for primary absolute and convective instabilities were obtained [3]. However, as soon as the threshold is exceeded the system enters a nonlinear regime where secondary instabilities arise leading to a more complex dynamics characterized by transition from dissipative periodic solutions to nonperiodic and/or chaotic ones.

In this paper we investigate these secondary instabilities in the presence of third-order dispersion and emphasize the crucial role of secondary convective and absolute instabilities in the dynamics of a coherently driven passive optical fiber cavity. Indeed, above threshold, dissipative time-modulated solutions are obtained. By increasing the incident pump power, these solutions destabilize and the system bifurcates either to a new periodic solution or enters a chaotic regime. At this stage a secondary instability threshold is reached. This threshold is crucial in the nonlinear dynamics of the system above threshold since it determines the stability range of the dissipative periodic solutions and subsequently the parameters range of their observation. An amplitude equation has been derived to describe the weakly nonlinear dynamics above the onset of instability that allows us to determine the threshold values for the different types of the secondary instability. An important result is that the threshold of absolute instability of modulated solutions determines the transition from modulated dissipative solutions to a regime of a temporal chaotic behavior [7].

II. THE MODEL

The system under investigation depicted in Fig. 1 can be modeled by the extended nonlinear Schrödinger equation with boundary conditions. This leads to a set of two equations, usually referred to as the map equations (or mapping) that can be reduced in the mean-field approximation to obtain a single equation modeling the intracavity field dynamics. This equation, known as the Lugiato-Lefever equation (LL model) [8], has been proven relevant for describing weakly nonlinear dynamics in cavities [9]. It reads

$$\frac{\partial \psi}{\partial t'} = S - (1 + i\Delta)\psi - is\frac{\partial^2 \psi}{\partial \tau'^2} + B_3\frac{\partial^3 \psi}{\partial \tau'^3} + i|\psi|^2\psi, \qquad (1)$$

where $t' = t\theta^2/2t_R$ is a slow normalized time variable, with t the real time and t_R the round-trip time, $\tau' = T\theta/(L|\beta_2|)^{1/2}$ is a fast normalized time variable, $s = \mathrm{sign}(\beta_2)$, $\psi = A(2\gamma L)^{1/2}/\theta$, $S = 2A_i(2\gamma L)^{1/2}/\theta^2$, $B_3 = \beta_3\theta/(3L^{1/2}|\beta_2|^{3/2})$, and $\Delta = 2\delta_0/\theta^2$. The amplitudes A_i and A are, respectively, slowly varying envelopes for the incident pump electric field and the intracavity electric field, δ_0 the cavity phase detuning, L the cavity length, γ the nonlinear

*saliya.coulibaly@univ-lille1.fr

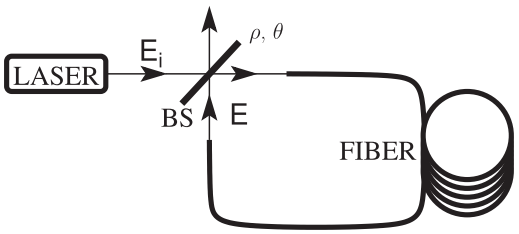

FIG. 1. Scheme of the fiber ring cavity (BS, beam splitter). ρ and θ are the amplitude reflection and transmission coefficients of BS ($\rho^2+\theta^2=1$).

coefficient of the fiber, and $\beta_{2,3}$ are the second-order and the third-order dispersion (TOD) terms respectively. The steady-state response ψ_s of Eq. (1) satisfies $S_s=[1+i(\Delta-|\psi_s|^2)]\psi_s$ so that the system is monostable (bistable) for $\Delta<\sqrt{3}$ ($\Delta>\sqrt{3}$). The linear stability analysis of the steady-state response with respect to finite frequency perturbations of the form $\exp[-i(Kt'-\Omega\tau')]$ shows that the primary threshold is reached at $I=I_s=1$ with $I=|\psi_s|^2$. Hence, the system evolves toward modulated solutions with the frequency $\Omega_c=\sqrt{(\Delta-2I_s)/s}$ associated to the wave number $k_c=B_3\Omega_c^3$.

III. THE AMPLITUDE EQUATION

To study the role of TOD in the nonlinear symmetry breaking of the generated traveling waves, and to keep mathematics as simple as possible, we perform a multiscale analysis similar to the one developed in [10] to find the amplitude equation describing the weakly nonlinear dynamics in the LL model. Beyond the primary threshold, the traveling wave solutions are assumed to take the form $\psi=\psi_s+a$, where a is a small perturbation. We expand this perturbation as $a=\varepsilon a_1+\varepsilon^2a_2+\varepsilon^3a_3+\cdots$, with ε a small parameter measuring the distance from the primary threshold: $\varepsilon^2=I-1$. Following the approach of [11], and taking into account the gain spectrum of the instability [9], we introduce the new times: $T_0=t$, $T_1=\varepsilon t$, $T_2=\varepsilon^2 t$, $\tau_0=\tau$, and $\tau_1=\varepsilon\tau$ so that the corresponding temporal derivatives become $\partial_t=\partial_{T_0}+\varepsilon\partial_{T_1}+\varepsilon^2\partial_{T_2}$ and $\partial_\tau=\partial_{\tau_0}+\varepsilon\partial_{\tau_1}$. By substitution of the above expansions in Eq. (1), we obtain a hierarchy of equations for the successive orders of ε. To the leading order we found $a_1=(1+i)[A_1e^{i(\Omega_c\tau'+k_ct')}+A_1^*e^{-i(\Omega_c\tau'+k_ct')}]$. The form of a_1 is justified by the fact that, right above the instability threshold, the gain is only positive in the vicinity of $\Omega=\pm\Omega_c$. A_1 and its complex conjugate A_1^* are slowly varying amplitudes, and the evolution of A_1 is described by the following equation, obtained by solving the system up to the third order:

$$\partial_{t'}S+3B_3\Omega_c^2\partial_{\tau'}S=\left(\psi_s^2-1\right)S+\left(2\Omega_c^2+3iB_3\Omega_c\right)\partial_{\tau'}^2S+(d_1+id_2)|S|^2S, \tag{2}$$

where we have set $S=\varepsilon A_1$ and the parameters are defined as

$$d_1=24\frac{2G+3}{G^2}+4\frac{G^2(1-2G)+H^2(2G-3)}{(G^2-H^2)^2+4H^2}, \tag{3}$$

$$d_2=\frac{4H[2(1-2G)+G^2-H^2]}{(G^2-H^2)^2+4H^2}, \tag{4}$$

with

$$G=3(\Delta-2),$$
$$H=-6B_3\Omega_c^3.$$

This equation of complex Ginzburg-Landau type [12] describes the time evolution of Stokes wave above the threshold. Here, an amplitude equation is derived above the threshold and takes into account both group velocity dispersion and TOD. Consequently, in the absence of TOD ($\beta_3=0$), three terms in Eq. (2) disappear since $B_3=0$ and $d_2=0$. Moreover, the expression of d_1 greatly simplifies to

$$d_1=\frac{30\Delta-41}{[3/2(\Delta-2)]^2} \tag{5}$$

and the numerator of d_1 shows clearly that the transition from super- to subcritical bifurcation is reached at $\Delta=41/30$ in agreement with the result in the seminal paper of Lugiato-Lefever [8]. As a result, the presence of TOD (β_3) drastically impacts the fiber cavity dynamics by introducing drift and diffraction effects [terms in Eq. (2) with $B_3\neq0$] together with a nonlinear frequency modulation (term with $d_2\neq0$). Note also that the presence of TOD affects the nature of the bifurcation [see Eq. (3)]. This issue is under investigation and it is out of the scope of this paper. In what follows, we consider values of β_3 in the parameter range where $d_1<0$ and consequently we deal with a supercritical bifurcation. In both convective and absolute regime, the instability domains are surrounded by the unstable trivial state. Here, we emphasize that while the trivial state is invaded by the modulational instability the envelope of the periodic solution obeys Eq. (2) and what we describe here is the dynamical behavior of this envelope, including the important issues such as its stability, characteristics (frequency, nature of the bifurcation, etc.), and the bifurcating solutions. This highlights the complex dynamics in the nonlinear regime. To this end, we seek solutions in the form

$$S_\omega=|S_\omega|e^{i(k_\omega t'+\omega\tau')}. \tag{6}$$

Substituting the above expression in Eq. (2) we obtained

$$|S_\omega|^2=\frac{1}{d_1}\left[2\Omega_c^2\omega^2-(I-1)\right], \tag{7}$$

$$k_\omega=-3B_3\Omega_c\omega^2-3B_3\Omega_c^2\omega+d_2|S_\omega|^2. \tag{8}$$

First, we consider solutions with $\omega=0$. In this case, the amplitude and the phase of modulated solutions are given by

$$|S_0|^2=-\frac{(I-1)}{d_1}, \tag{9}$$

$$k_0=-\frac{d_2(I-1)}{d_1}. \tag{10}$$

Hence, the corresponding solution in the LL model can be written as

$$\psi_0=\psi_s+(1+i)|S_0|[e^{i[\Omega_c\tau'+(k_c+k_0)t']}+e^{-i[\Omega_c\tau'+(k_c+k_0)t']}]. \tag{11}$$

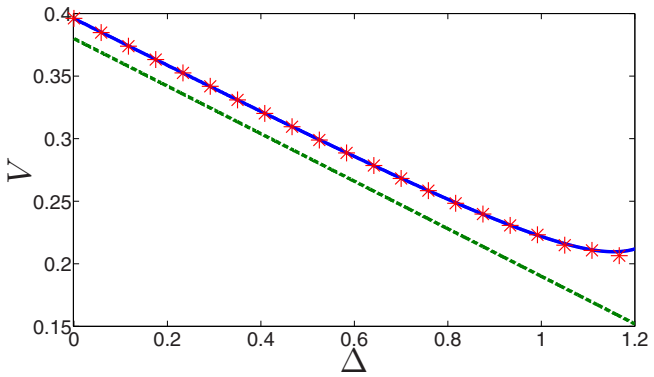

FIG. 2. (Color online) Analytical velocity given by Eq. (12) (solid blue line) as a function of the detuning parameter compared with numerical results from the LL model (red stars) for $I = 1.1$, $s = -1$, and $B_3 = -0.19$. The green dashed line corresponds to the result of the linear analysis [first term on the right-hand side of Eq. (12)].

This expression describes the main modulated solution with a maximum MI gain appearing beyond the primary threshold. A first interesting result is that the TOD introduces a phase term k_0 depending linearly on the intracavity field above threshold $(I - 1)$. Therefore, the phase velocity of the modulated solution is given by [10]

$$V = \frac{k_c + k_0}{\Omega_c} = V_c - \frac{d_2}{\Omega_c d_1}(I - 1), \tag{12}$$

where $V_c = k_c/\Omega_c = -B_3\Omega_c^2$ is the phase velocity at threshold. The dependence of the velocity on the control parameter has already been reported in the complex Ginzburg-Landau-type equation (see, e.g., [10]). Here, we emphasize that this dependence induces nontrivial variation of the velocity with respect to the other parameters. Indeed, considering, for example, the dependence on the detuning parameter, the standard analysis gives a linear evolution (dashed green line in Fig. 2). However, as can be seen from Fig. 2 which displays the velocity given by the numerical simulations with respect to the detuning Δ (stars), the variation is not linear. On the same figure we have plotted Eq. (12) (solid line) which displays a very good agreement with the numerical results.

IV. THE ECKHAUS-BENJAMIN-FEIR INSTABILITY

So far, we focused on the solution S_0. However, according to the relation (7), more solutions S_ω may appear for $(I - 1) > 2\Omega_c^2\omega^2$ since $d_1 < 0$. We will show in this section that some of these solutions are unstable to perturbations of the form $e^{i\delta\omega t'}$. This instability is called the Eckhaus instability in the case of stationary waves corresponding to $B_3 = 0$ ($\beta_3 = 0$) and the Benjamin-Feir instability in the case of progressive waves corresponding to $B_3 \neq 0$ ($\beta_3 \neq 0$) [12]. To simplify analytical calculations it is more convenient to normalize Eq. (2) as

$$\frac{\partial\tilde{S}}{\partial\tilde{t}} = \tilde{S} + (1 + ib)\frac{\partial^2\tilde{S}}{\partial\tilde{\tau}^2} - (1 + ic)|\tilde{S}|^2\tilde{S}, \tag{13}$$

with

$$\begin{aligned}
\tilde{S} &= \sqrt{\frac{-d_1}{\varepsilon^2}}S,\\
\tilde{t} &= \varepsilon^2 t',\\
\tilde{\tau} &= \sqrt{\frac{\varepsilon^2}{2\Omega_c^2}}\left(\tau' - 3B_3\Omega_c^2 t'\right),\\
b &= \frac{3B_3}{2\Omega_c},\\
c &= \frac{d_2}{d_1}.
\end{aligned} \tag{14}$$

The modulated solutions of Eq. (13) take the following form:

$$\tilde{S}_{\tilde{\omega}} = \sqrt{1 - \tilde{\omega}^2}e^{i(\tilde{\omega}\tilde{\tau} - \tilde{k}_{\tilde{\omega}}\tilde{t})}, \tag{15}$$

with

$$\tilde{k}_{\tilde{\omega}} = c(1 - \tilde{\omega}^2) + b\tilde{\omega}^2. \tag{16}$$

Obviously, the solution (15) can only exist for

$$\tilde{\omega}^2 < 1. \tag{17}$$

We perform the linear stability analysis of the solution (15) by injecting in Eq. (13) a solution in the form

$$\tilde{S} = (|\tilde{S}_{\tilde{\omega}}| + \delta a)e^{i(\tilde{\omega}\tilde{\tau} - \tilde{k}_{\tilde{\omega}}\tilde{t})}, \tag{18}$$

with

$$\delta a = \delta a_+ e^{(\lambda\tilde{t} + iq\tilde{\tau})} + \delta a_- e^{(\lambda^*\tilde{t} - iq\tilde{\tau})}. \tag{19}$$

Then we obtain the following dispersion relation [13]:

$$\begin{aligned}
\lambda = &-|\tilde{S}_{\tilde{\omega}}|^2 - 2ibq\tilde{\omega} - q^2\\
&+\sqrt{(1 + c^2)|\tilde{S}_{\tilde{\omega}}|^4 - (bq^2 - 2i\tilde{\omega}q + c|\tilde{S}_{\tilde{\omega}}|^2)^2}.
\end{aligned} \tag{20}$$

A. The Eckhaus instability ($b = c = 0$)

First, we consider the case where the TOD term is absent ($b = c = 0$). From Eq. (15), the corresponding form of the modulated solution can be written as

$$\tilde{S}_{\tilde{\omega}} = \sqrt{1 - \tilde{\omega}^2}e^{i\tilde{\omega}\tilde{\tau}} \tag{21}$$

and λ [expression (20)] takes a simpler form

$$\lambda_E = -|\tilde{S}_{\tilde{\omega}}|^2 - q^2 + \sqrt{|\tilde{S}_{\tilde{\omega}}|^4 + 4\tilde{\omega}^2q^2}. \tag{22}$$

The analysis of the real part of λ_E shows that the solution (21) is unstable for

$$\tilde{\omega}^2 > \tfrac{1}{3}. \tag{23}$$

The most unstable mode $q_{\max}$ is calculated from the relation $(\partial\,\mathrm{Re}[\lambda_E]/\partial q)|_{q_{\max}} = 0$, and it takes the following form:

$$q_{\max}^2 = \tfrac{3}{4}\left(\tilde{\omega}^2 - \tfrac{1}{3}\right)(1 + \tilde{\omega}^2)\tilde{\omega}^{-2}. \tag{24}$$

We note that $q_{\max} \to 0$, when $\tilde{\omega} \to 1/3$ and $q_{\max} \to 1$, when $\tilde{\omega} \to 1$.

This instability is known as the Eckhaus instability. It has been extensively studied in fluid mechanics as, for instance, in the case of cells of Rayleigh-Benard convection (see [14], and references therein) and also in optics [15]. When the frequency

of the modulated solution satisfies the criterion (23), this instability causes the disappearance of the initial modulation at frequency $\tilde{\omega}$ and the amplification of a frequency domain around the most unstable frequency $\tilde{\omega} - q_{\max}$ ($\tilde{\omega} + q_{\max}$) in the case of $\tilde{\omega} > 0$ ($\tilde{\omega} < 0$). Numerical simulations obtained by integrating Eq. (13) for a stable frequency ($\tilde{\omega} = 1/2$) and an unstable frequency ($\tilde{\omega} = \sqrt{2/3}$) are shown in Fig. 3. In this example, Figs. 3(a) and 3(b) show clearly the stability of the modulated solution with $\tilde{\omega} = 1/2$. For the case of $\tilde{\omega} = \sqrt{2/3} \approx 0.81$, the above calculations show that it is unstable to the modulations q around the most unstable mode $q_{\max} = 5/8 \approx 0.79$, the predicted frequency of the bifurcated solution is $\tilde{\omega} - q_{\max} \approx 0.02$, close to zero with a slow period $2\pi/(\tilde{\omega} - q_{\max}) \approx 300$. As can be seen from Fig. 3(d) numerical results are in excellent agreement both qualitatively and quantitatively with the predictions. Since the Eckhaus instability is found in the normalized amplitude equation [Eq. (13)], it is interesting to check this instability in the LL model (1). By using the relations (14), we can obtain a relation that connects the normalized frequency $\tilde{\omega}$ to the frequency ω in the LL model as

$$\omega^2 = \frac{\varepsilon^2}{2\Omega_c^2}\tilde{\omega}^2, \tag{25}$$

where $\varepsilon^2 = I - 1$. Using (25), we can also express the existence condition of modulated solutions ($\tilde{\omega}^2 < 1$) and their stability condition ($\tilde{\omega}^2 < \frac{1}{3}$) in the parameters of the LL model as

$$\varepsilon^2 > 2\omega^2\Omega_c^2, \tag{26}$$

$$\varepsilon^2 > 6\omega^2\Omega_c^2. \tag{27}$$

In Fig. 4 we show the domain where the Eckhaus instability is possible in the LL model (green area). The unstable domain is bounded by the solid black line and the dotted blue line. To observe the Eckhaus instability in the LL model, we must first find the form of the modulated solution (21) related to this model. Using the relations (14), we found

$$\psi_\omega = \psi_s + (1+i)\frac{|\tilde{S}_{\tilde{\omega}}|}{\sqrt{-d_1}}[e^{i[(\Omega_c+\omega)\tau' + k_c t']} + e^{-i[(\Omega_c+\omega)\tau' + k_c t']}]. \tag{28}$$

In Fig. 5 we present the result of a numerical simulation in the LL model [Eq. (1)] seeded by an initial condition that satisfies Eq. (28). This initial signal has two frequencies at $\Omega_c + \omega$ and $-\Omega_c - \omega$ [Fig. 5(a)]. During the propagation, we observe the attenuation of the two initial frequencies and the amplification of two spectral sidebands around the frequencies $\Omega_{\max} = \Omega_c + \omega - Q_{\max}$ and $-\Omega_{\max} = -\Omega_c - \omega + Q_{\max}$ with $Q_{\max}^2 = q_{\max}^2\varepsilon^2/2\Omega_c^2$ corresponding to the most unstable mode (the Eckhaus mode). In Fig. 5(b), the numerical most unstable frequencies (blue solid line) caused by the Eckhaus instability are close but slightly different from the positions calculated analytically (red dotted line). Two factors contribute to this slight disagreement: First, we have limited the calculation to the first order in ε to find the solution in the LL model; second, since the multiscale calculation is performed with $I - I_s$ small, the result can be very sensitive to the values of I in the numerical integration of the LL model.

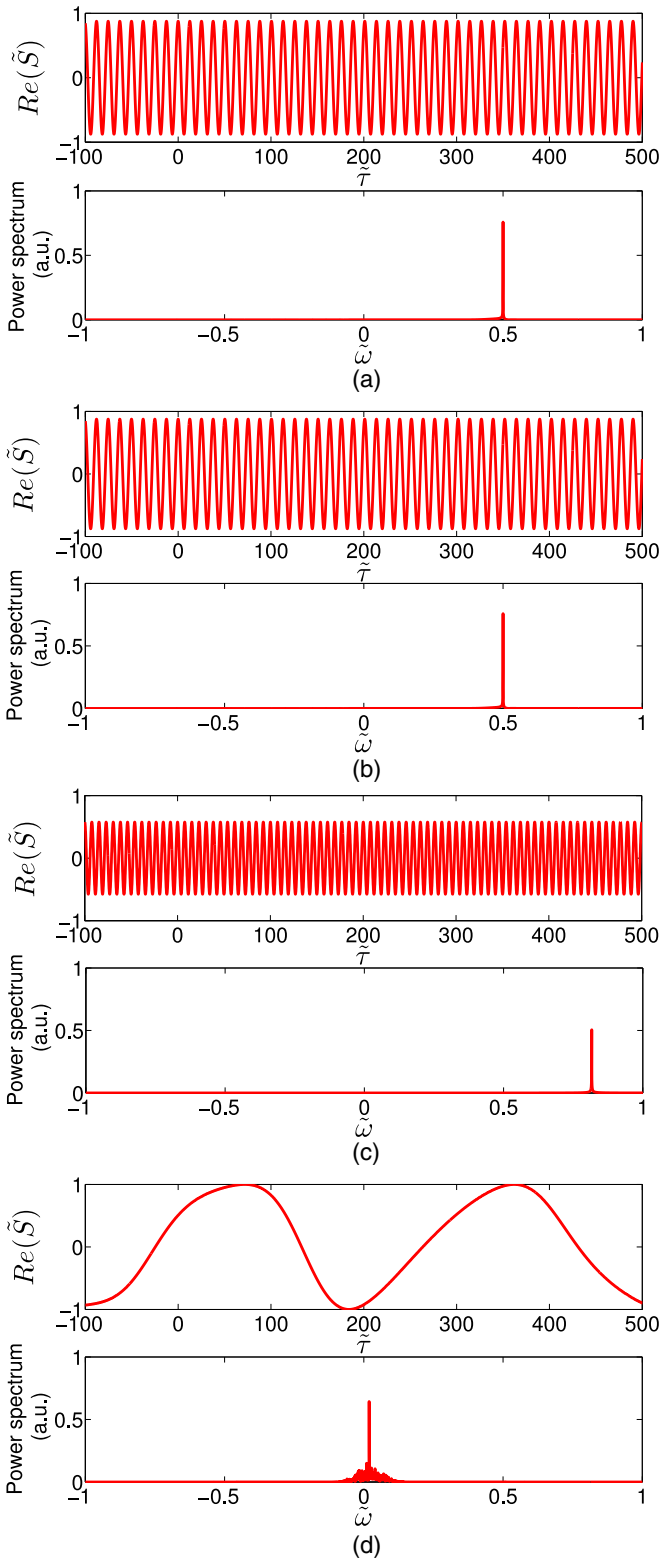

FIG. 3. (Color online) The real part of the signals in time and frequency domains. (a) and (b) show the initial and final (at $\tilde{t} = 1000$) signal with a frequency $\tilde{\omega} = \sqrt{1/4}$ in the stability range and (c) and (d) show the initial and final (at $\tilde{t} = 1000$) signals with a frequency $\tilde{\omega} = \sqrt{2/3}$ in the instability range.

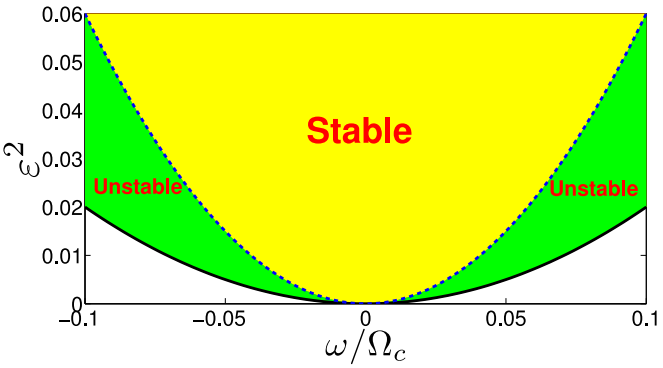

FIG. 4. (Color online) Zone of instability in the ω/Ω_c-ε^2 plane. The relation $\varepsilon^2 = 2\omega^2\Omega_c^2$ is represented by the solid black curve defining the region where the modulated solution can exist and the relation $\varepsilon^2 = 6\omega^2\Omega_c^2$ is represented by the dotted blue curve which delimits the region of stable solutions with $s = -1$, $\Delta = 1$, and $\Omega_c = 1$.

B. The Benjamin-Feir instability ($b \neq 0$, $c \neq 0$)

When the TOD is present in our model, the parameters b and c of Eq. (13) are both nonzero. Therefore, the dynamics of our system becomes more complex. The TOD induced a drift

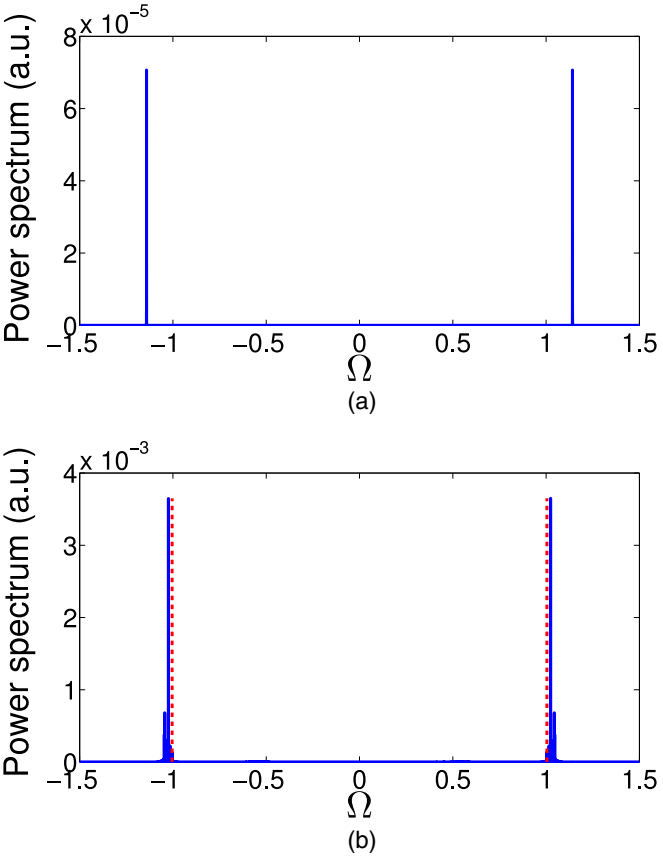

FIG. 5. (Color online) (a) The initial spectrum of the signal ψ_ω and (b) the spectrum of ψ_ω at $t' = 2500$ of a simulation in the LL model with $\tilde{\omega} = \sqrt{2/3}$, $s = -1$, $\Delta = 1$, $I = 1.06$, and $\Omega_c = 1$. The red dotted line in (b) indicates the predicted positions of $\Omega_{\max}$ and $-\Omega_{\max}$.

to modulated solutions that are stationary in the case of $b = 0$ and $c = 0$ [i.e., $\tilde{k}_{\tilde{\omega}} = 0$ in Eq. (29) below]. This drift gives rise to the appearance of two types of instability regimes of modulated solutions: a convective regime and an absolute one. We start by rewriting the modulated solution in its complete form

$$\tilde{S}_{\tilde{\omega}} = \sqrt{1-\tilde{\omega}^2}\, e^{i(\tilde{\omega}\tilde{\tau} - \tilde{k}_{\tilde{\omega}}\tilde{l})} \tag{29}$$

with

$$\tilde{k}_{\tilde{\omega}} = c(1-\tilde{\omega}^2) + b\tilde{\omega}^2.$$

The phase drift velocity of solution (29) is given by $\tilde{v} = \tilde{k}_{\tilde{\omega}}/\tilde{\omega}$. Note that $\tilde{v}$ may be positive or negative depending on the values of b, c, and $\tilde{\omega}$. The analysis of the eigenvalue λ [expression (20)] allows one to understand the dynamics in different instability regimes of solution (29). For the sake of simplicity, we develop λ for $q \to 0$ to obtain an approximate expression as follows [12,13]:

$$\lambda_a = -iV_g q - Dq^2 + O(q^3) \tag{30}$$

with

$$V_g = 2(b-c)\tilde{\omega}, \tag{31}$$

$$D = 1 + bc - \frac{2(1+c^2)\tilde{\omega}}{1-\tilde{\omega}^2}. \tag{32}$$

The approximate expression of λ [expression (30)] allows us to get good insight into the stability of solution (29). Indeed, the sign of D determines the stability of this solution: It is stable ($\mathrm{Re}[\lambda_a] < 0$) when $D > 0$. Using expression (32), we can express the stability criterion as

$$\tilde{\omega}^2 < \frac{1+bc}{3+2c^2+bc}. \tag{33}$$

Notice that, condition (23) is recovered when setting $b = c = 0$. The solution $\tilde{S}_0$ (solution corresponding to $\tilde{\omega} = 0$) is stable if the Benjamin-Feir-Newell criterion $1 + bc > 0$ is satisfied [12]. The most unstable mode (the Eckhaus mode) can be found by using the following relation:

$$\left.\frac{\partial\, \mathrm{Re}[\lambda]}{\partial q}\right|_{q_{\max}} = 0. \tag{34}$$

From the approximate expression of the eigenvalue λ_a we obtain $q_{\max} = 0$. In the study of the convective and absolute instability, the relation $\tilde{\omega}^2 = (1+bc)/(3+2c^2+bc)$ determines the convective threshold. However, the approximate expression of λ_a is not sufficient to predict the absolute threshold and the most unstable mode (the Eckhaus mode) beyond the convective threshold; we then consider the exact expression of λ [Eq. (20)] to continue the analysis. Indeed, in the general context of convective and absolute instabilities, λ and q are both complex as $\lambda = \mathrm{Re}[\lambda] + i\,\mathrm{Im}[\lambda]$ and $q = \mathrm{Re}[q] + i\,\mathrm{Im}[q]$. By replacing these two complex terms in the exponential part of the perturbation [Eq. (19)], we found

$$\delta a \propto e^{(\lambda\tilde{l} + iq\tilde{\tau})} = e^{[\mathrm{Re}[\lambda] - \mathrm{Im}[q](\tilde{\tau}/\tilde{l})]\tilde{l}} e^{i[Im[\lambda] + \mathrm{Re}[q](\tilde{\tau}/\tilde{l})]\tilde{l}}. \tag{35}$$

Here, we define the drift V and the total growth rate σ of the perturbation as follows [16]:

$$V = \frac{\tilde{\tau}}{\tilde{t}}, \tag{36}$$

$$\sigma = \mathrm{Re}[\lambda] - \mathrm{Im}[q]V, \tag{37}$$

where the total gain σ represents the temporal growth rate along each drift V. The asymptotic dominant frequencies q_s are defined by the saddle-point method [16–18],

$$\partial_q \lambda(q_s) = V(q_s). \tag{38}$$

The absolute threshold is reached when the following conditions are satisfied [12,13,16]:

$$\partial_q \lambda(q_{sa}) = 0, \tag{39}$$

$$\mathrm{Re}[\lambda(q_{sa})] = 0. \tag{40}$$

The frequency q_{sa} is commonly called the absolute frequency. By solving numerically Eqs. (39) and (40), we can express the absolute threshold as a function of b, c, and $\tilde{\omega}$. An example is given in Fig. 6(a), following the same method as in [12]. The black dashed line represents the absolute threshold in the plane ($\tilde{\omega}$,c) for $b = -1.5$. A path with $\tilde{\omega} = 0.3$ (blue dashed line) is chosen to test the convective and absolute thresholds obtained. This path intersects the convective threshold curve at $c_c = 0.5$ and the absolute threshold curve at $c_a = 1.05$. Figure 6(b) shows the total gain versus V for five values of c with $\tilde{\omega} = 0.3$ and $b = -1.5$ to examine the transition between the different regimes. When $c \leqslant c_c$ (stable regime), the modulated solution (29) is stable, the total gain is negative for all V except one drift V with $\sigma = 0$ which corresponds to the drift of the stable modulated solution [see the curve labeled $c = 0.1$ in Fig. 6(b)], and it is marginally stable. By increasing c, the total gain curve does not move vertically but horizontally; this means that the modulated solution is always stable but its drift can change depending on c [see the curves labeled $c = 0.1$ and $c = 0.5$ in Fig. 6(b)]. Just above the convective threshold, the total gain curve rises vertically with increasing c leading to a range of unstable V with σ positive [see the curve labeled $c = 0.8$ in Fig. 6(b)]. In this regime $\sigma(V)$ is positive but only for negative values of V. This means that the perturbation grows only in one direction and the solution (29) is convectively unstable. At the absolute threshold, the limit of the positive part of the total gain curve ($\sigma = 0$) reaches $V = 0$ [see the curve labeled $c_a = 1.05$ in Fig. 6(b)]. By increasing c, the positive part of the total gain curve extends simultaneously in the range of $V < 0$ and $V > 0$ [see the curve labeled $c = 1.3$ in Fig. 6(b)] and the perturbation develops in both directions so that the solution (29) is absolutely unstable. Before going further, we would like to emphasize that the splitting of the secondary instabilities on convective and absolute regimes is induced here by the TOD, in contrary to previous works in hydrodynamics and optics where the splitting results from a drift term (first derivative).

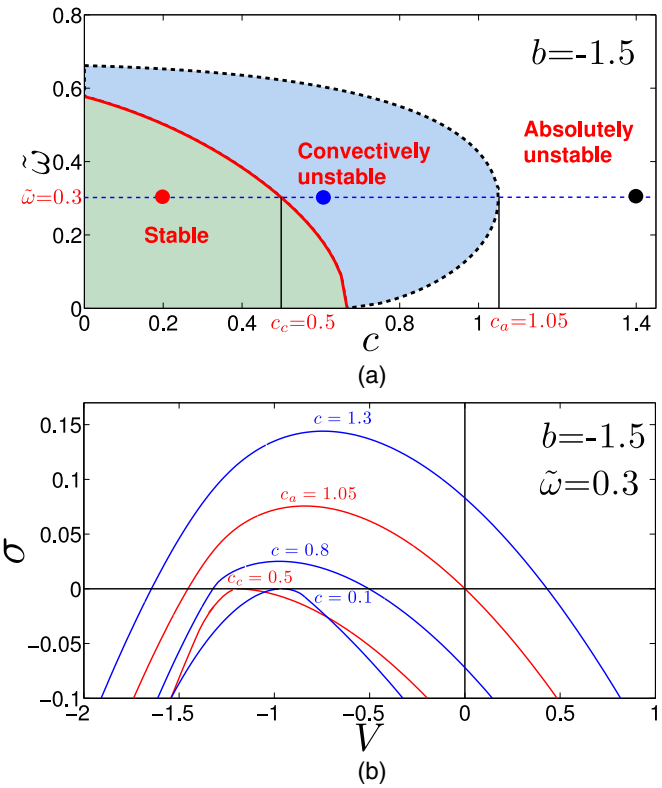

FIG. 6. (Color online) (a) The convective and absolute instabilities in the $\tilde{\omega}$-c plane with $b = -1.5$. The solid red line represents the limit of the Eckhaus instability $\tilde{\omega}^2 = (1 + bc)/(3 + bc + 2c^2)$ for $q \to 0$ and the dashed black curve shows the marginal curve which separates the zone of the convective and absolute instabilities; it is obtained from the relations (39) and (40). (b) The total growth rate σ (gain) versus V for five values of c.

We have performed three numerical simulations by integrating Eq. (13) to distinguish these different regimes: the first one in the stable regime, the second in the convective regime, and the last in the absolute regime. These simulations are denoted by circles in Fig. 6(a) with red ($c = 0.2$), blue ($c = 0.6$), and black ($c = 1.4$), respectively. In all simulations, we superimposed a localized perturbation to the solution (29) around the position $\tilde{\tau} = 0$ as an initial condition [Figs. 7(b), 8(b), and 9(b)], and follow its evolution. In the stable regime, the localized perturbation drifts in the $\tilde{\tau}$-$\tilde{t}$ plane as shown in Fig. 7(a) where the drift of the perturbation is given by $V = V_g = 2(b - c)\tilde{\omega}$. Note that the black and white fringes represent the oscillation of the modulated solution at frequency $\tilde{\omega} = 0.3$. Indeed, the slope of the fringes in the $\tilde{\tau}$-$\tilde{t}$ plane means that the modulated solution drifts itself along $\tilde{\tau}$ with a phase velocity $v = \tilde{k}_{\tilde{\omega}}/\tilde{\omega}$. In the temporal profiles and the spectrum of the signal at $\tilde{t} = 300$ [Fig. 7(c)] and $\tilde{t} = 600$ [Fig. 7(d)], we observe that the perturbation is lessened and the system returns to the stable modulated solution (the positions of the perturbation are framed by the black dotted rectangles). In the convective regime, the evolution of the signal in the $\tilde{\tau}$-$\tilde{t}$ plane is displayed in Fig. 8(a) where we observe that the affected part of the signal by the initial perturbation extends and drifts only in the backward direction during the simulation, and it completely leaves the observation domain under the effect of the drift at $\tilde{t} = 500$. Note that the drift is negative as shown in Fig. 6(b). The temporal profiles and the spectra show that the affected part of the signal tends to form an oscillation of the Eckhaus frequency [Fig. 8(c)], but this frequency

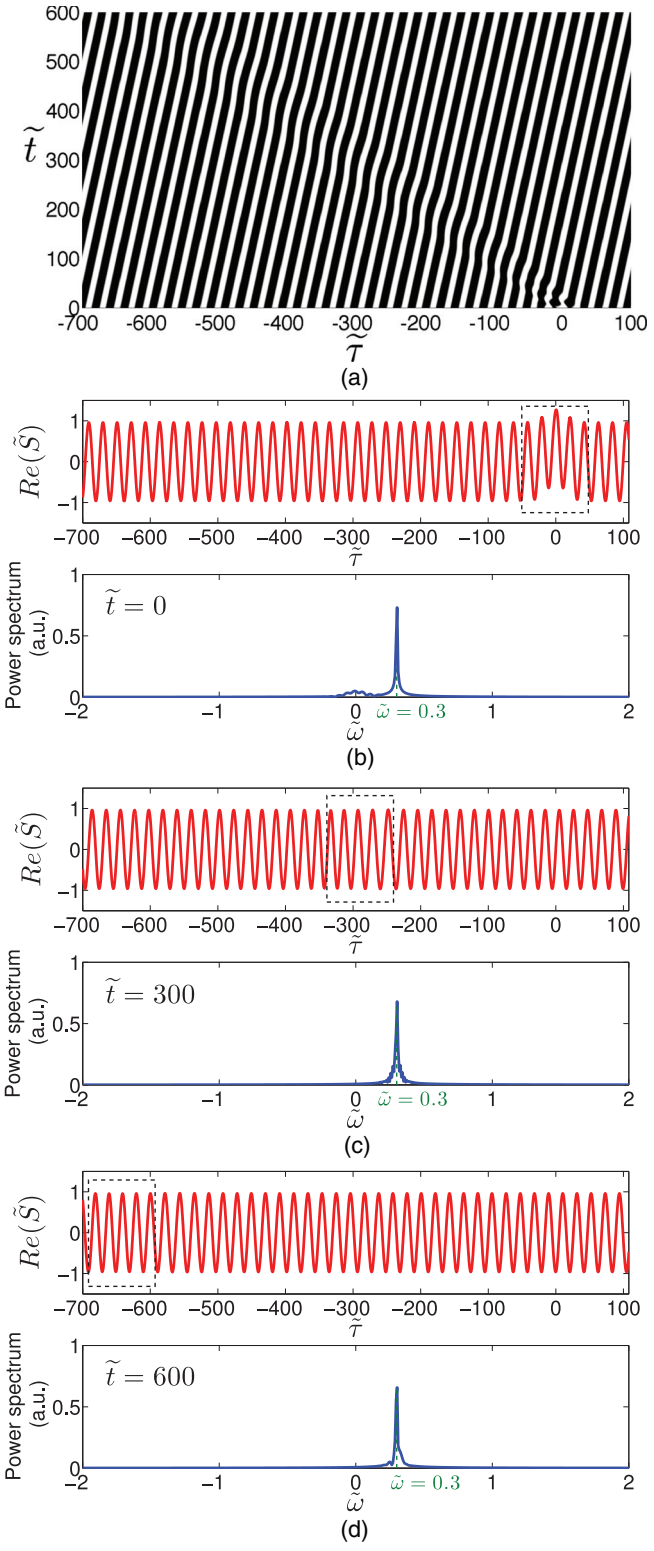

FIG. 7. (Color online) Numerical simulations obtained by integrating the normalized amplitude equation [Eq. (13)] in a stable case. (a) The evolution of a perturbation initially located at $\tilde{\tau} = 0$ on the modulated solution in the $\tilde{\tau}$-$\tilde{t}$ plane.(b), (c), and (d) represent, respectively, the temporal profiles and the spectra of the signal at $\tilde{t} = 0$, $\tilde{t} = 300$, and $\tilde{t} = 600$ with $\tilde{\omega} = 0.3$, $b = -1.5$, and $c = 0.2$.

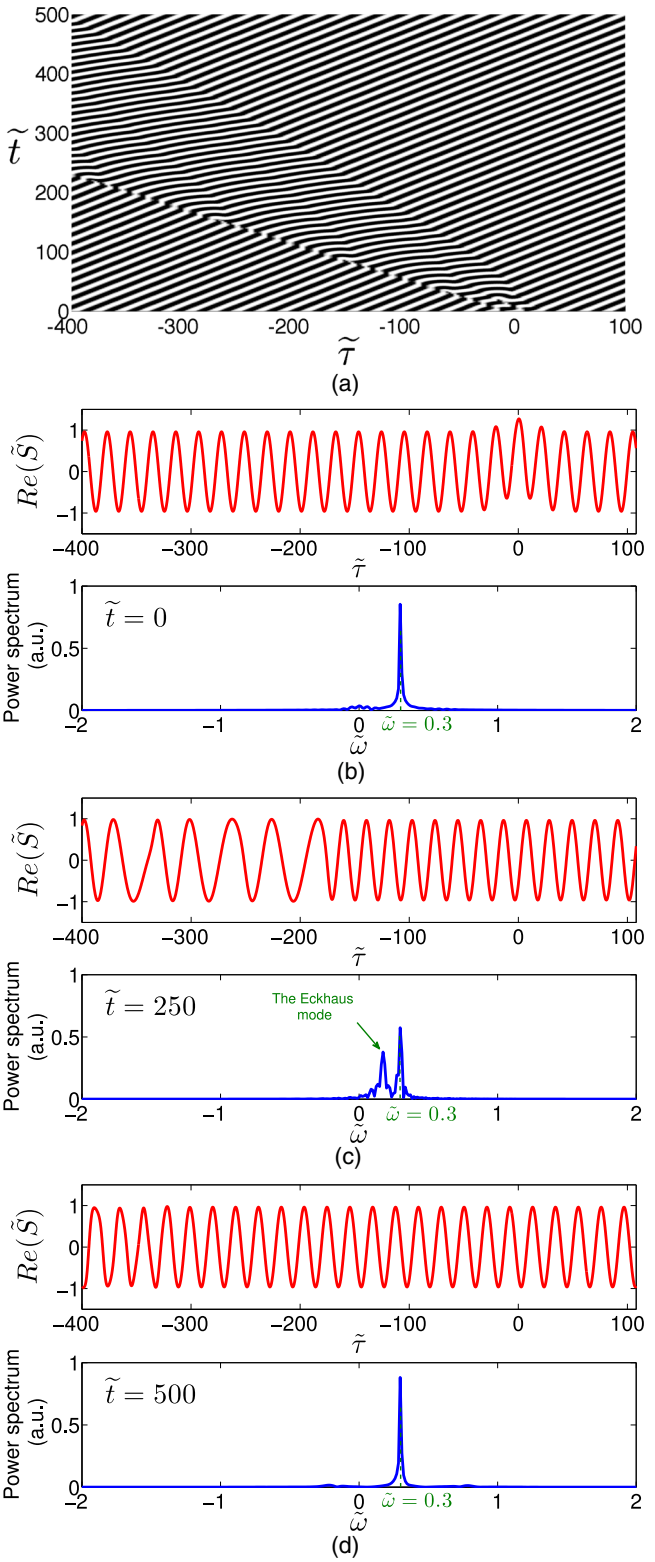

FIG. 8. (Color online) Numerical simulations obtained by integrating the normalized amplitude equation [Eq. (13)] in the convective regime. (a) The evolution of a perturbation initially located at $\tilde{\tau} = 0$ on the modulated solution in the $\tilde{\tau}$-$\tilde{t}$ plane. (b), (c), and (d) represent, respectively, the temporal profiles and the spectra of the signal at $\tilde{t} = 0$, $\tilde{t} = 250$, and $\tilde{t} = 500$ with $\tilde{\omega} = 0.3$, $b = -1.5$, and $c = 0.6$.

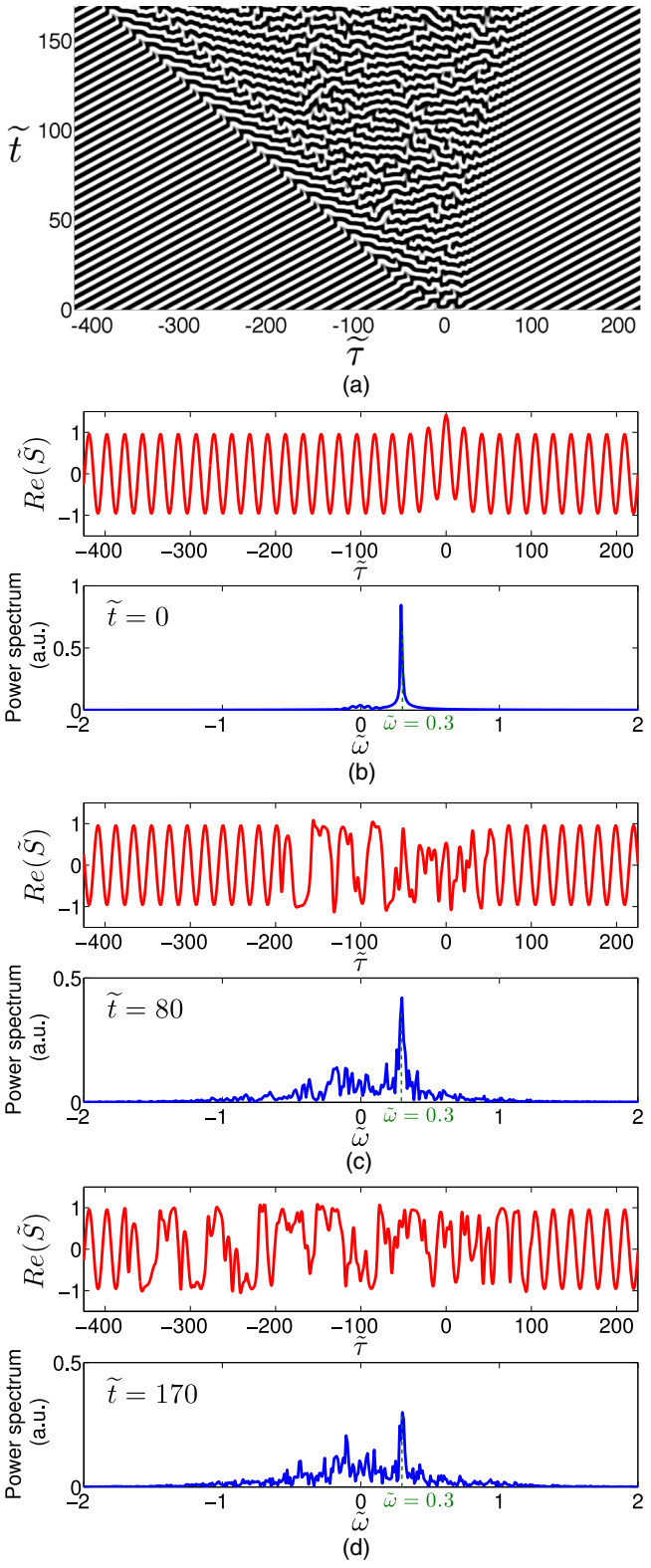

FIG. 9. (Color online) Numerical simulations obtained by integrating the normalized amplitude equation [Eq. (13)] in the absolute regime. (a) The evolution of a perturbation initially located at $\tilde{\tau} = 0$ on the modulated solution in the $\tilde{\tau}$-$\tilde{t}$ plane. (b), (c), and (d) represent, respectively, the temporal profiles and the spectra of the signal at $\tilde{t} = 0$, $\tilde{t} = 80$, and $\tilde{t} = 170$ with $\tilde{\omega} = 0.3$, $b = -1.5$, and $c = 1.4$.

eventually disappears and the spectrum finds its initial state after the perturbed part of the signal completely leaves the observation domain under the effect of the drift [Fig. 8(d)]. This is in excellent agreement with our analytical prediction about the existence of a convective regime where the system asymptotically recovers its initial state. In the absolute regime, the evolution of the signal in the $\tilde{\tau}$-$\tilde{t}$ plane is shown in Fig. 9(a) where the perturbation affects all the signals and it finally invades the entire observation domain. During the evolution, the initial frequency $\tilde{\omega}$ disappears, but we do not observe the amplification of the Eckhaus frequency and the affected part of the signal loses completely the modulated form [Figs. 9(c) and 9(d)]. Note that a similar behavior has been reported in [7]. The authors investigated transition from periodic oscillations to spatiotemporal chaos in a classic ecological system of invasion of prey population by predators. Here, in addition to the concept of convective and absolute instability, an advanced nonlinear study is necessary to explain our results by taking into account the interactions between all unstable modes and their relative stabilities.

After investigating the nonstationary modulated solutions and their stabilities in the normalized amplitude equation [Eq. (13)], let us return to the LL model [Eq. (1)]. In fact, the nature of the instability depends directly on the frame of reference in which we observe the instability: it can be convective in a frame of reference and absolute in another one. The key factor here is the drift of the frame of reference we chose. In our case, we first need to reconsider the normalization [Eq. (14)] which connects the time variable τ' of the LL model to the normalized variable $\tilde{\tau}$ as

$$\tau' = \sqrt{\frac{2\Omega_c^2}{\varepsilon^2}}\left(\tilde{\tau} - \frac{3B_3\Omega_c}{\sqrt{2}\varepsilon}\tilde{t}\right). \tag{41}$$

We found that the frame of reference of the LL model is moving in the frame of reference of the normalized amplitude equation with a drift $3B_3\Omega_c/\sqrt{2}\varepsilon$ that we note V_c. We also introduce the drifts of the limiting fronts of the wave packet in the normalized amplitude equation [Eq. (13)]. These fronts are marginally stable and defined by $\sigma(V_-) = \sigma(V_+) = 0$ where V_- and V_+ represent the drift of the leading and the trailing edges, respectively. According to the concept of convective and absolute instability applied to propagating wave packets in unstable medium [19], the instability of the modulated solution is absolute in the LL model if $(V_- - V_c)(V_+ - V_c) < 0$, otherwise, it is convective. However, with parameters in our analysis, V_+ and V_- are always smaller than V_c, leading to a convective regime in the LL model.

V. CONCLUSION

In summary, we studied analytically and numerically the impact of the TOD on modulated solutions that appear above the onset of instability in a fiber ring cavity. We have shown that the presence of the TOD induced a drift which leads to the appearance of convective and absolute instability regimes of the modulated solution in the amplitude equation. In the convective regime, we numerically show that a localized perturbation impacts the modulated solution by shifting its modulation frequency to the Eckhaus frequency.

Under the effect of the drift, the modulated solution recovers its initial state after the localized perturbation completely leaves the observation domain. In the absolute regime, the localized perturbation affects all modulated solutions, but we do not observe the appearance of the Eckhaus frequency. The modulated solution completely loses the modulated form and enters a chaotic regime. A nonlinear advanced study is needed to explain this result and will be a prospect for future work. Our analytical and numerical studies of the amplitude equation led us to conclude that the instability of modulated solutions in the LL model is convective according to the range of physical parameters explored in this study.

ACKNOWLEDGMENTS

This work is supported by the Belgian Science Policy Office (BelSPO) under Grant No. IAP 7-35, French Ministry of Higher Education and Research, the French Project "ANR Blanc N12-BS04-0011-02", and the French Labex CEMPI (ANR-11-LABX-0007-01).

[1] M. Tlidi, M. Taki, and T. Kolokolnikov, Chaos **17**, 037101 (2007).
[2] N. Akhmediev and A. Ankiewicz, *Dissipative Solitons: From Optics to Biology and Medicine* (Springer-Verlag, Berlin, Heidelberg, 2008).
[3] A. Mussot, E. Louvergneaux, N. Akhmediev, F. Reynaud, L. Delage, and M. Taki, Phys. Rev. Lett. **101**, 113904 (2008).
[4] F. Leo, S. Coen, P. Kockaert, S.-P. Gorza, P. Emplit, and M. Haelterman, Nat. Photonics **4**, 471 (2010).
[5] A. Mussot, A. Kudlinski, E. Louvergneaux, M. Kolobov, and M. Douay, Phys. Lett. A **374**, 691 (2010).
[6] F. Leo, A. Mussot, P. Kockaert, P. Emplit, M. Haelterman, and M. Taki, Phys. Rev. Lett. **110**, 104103 (2013).
[7] J. A. Sherratt, M. J. Smith, and J. D. M. Rademacher, Proc. Natl. Acad. Sci. USA **106**, 10890 (2009).
[8] L. A. Lugiato and R. Lefever, Phys. Rev. Lett. **58**, 2209 (1987).
[9] M. Haelterman, S. Trillo, and S. Wabnitz, Opt. Commun. **91**, 401 (1992).
[10] R. Zambrini, M. San Miguel, C. Durniak, and M. Taki, Phys. Rev. E **72**, 025603 (2005).
[11] P. Manneville, *Instabilities, Chaos and Turbulence* (Imperial College Press, London, 1994).
[12] I. S. Aranson and L. Kramer, Rev. Mod. Phys. **74**, 99 (2002).
[13] I. S. Aranson, L. Aranson, L. Kramer, and A. Weber, Phys. Rev. A **46**, R2992 (1992).
[14] M. C. Cross and P. C. Hohenberg, Rev. Mod. Phys. **65**, 851 (1993).
[15] M. Taki, M. N. Ouarzazi, H. Ward, and P. Glorieux, J. Opt. Soc. Am. B **17**, 997 (2000).
[16] P. Huerre and P. A. Monkewitz, Annu. Rev. Fluid Mech. **22**, 473 (1990).
[17] C. Bender and S. Orszag, *Advanced Mathematical Methods for Scientists and Engineers* (MacGraw-Hill, New York, 1978).
[18] H. Ward, M. N. Ouarzazi, M. Taki, and P. Glorieux, Phys. Rev. E **63**, 016604 (2000).
[19] G. S. Triantafyllou, Phys. Fluids **6**, 164 (1993).